npj | flexible electronics

www.nature.com/npjflexelectron

ARTICLE OPEN

Check for updates

Ultrahigh-transparency and pressure-sensitive iontronic device for tactile intelligence

Jie Tang[1,2], Chao Zhao[2], Qian Luo[2,3], Yu Chang[2,3]✉, Zhenguo Yang[1]✉ and Tingrui Pan[3,4]✉

Emerging tactile sensing devices mimic biological functions of human mechanoreception. By introducing the feature of optical transparency, it can lead to a combined capacities of tactile and visual intelligence into single system. Yet, it is difficult to realize ultrahigh level of optical transparency and device sensitivity in single structure, for the widely used methods for sensitivity improvement, such as elevating the interfacial roughness, may further reduce the transparency. By utilizing a transparent ionic material with tunable surface topologies, as well as introducing a strategy of refractive index matching, we have proposed a transparent iontronic sensing (TIS) device based on the iontronic sensing mechanism, simultaneously offering combined high device sensitivity (83.9 kPa^{-1}), with ultrahigh optical transparency (96.9%), the highest reported value in literature. Benefiting from its comprehensive performance in sensing and optical characteristics, the TIS devices hold enormous potential for the human-machine interfaces for industrial and medical applications.

npj Flexible Electronics (2022)6:54 ; https://doi.org/10.1038/s41528-022-00162-y

INTRODUCTION

Tactile sensation, representing an important perceptive and intelligence-collecting function for human beings, has been an active topic of research and development in recent years[1,2]. In order to obtain the desired touch information, flexible tactile sensing technologies have been frequently sought to accomplish this analog-to-digital conversion process, which simulates the biological functions of tactile perception[3]. As a key performance characteristic, the device sensitivity serves a major consideration for the tactile sensor design, evaluating the sensing capacity under the minimal pressure variations resolvable[3]. With the high device sensitivity, the tactile sensor has enabled specific applications, such as touch and gesture recognition and physiological signal detection[4]. Recent technological trend in sensor fusing and multimodality detection provides additional incentives to enabling special features to the existing schemes. To this end, incorporating optical properties into the tactile sensors could lead to more functionalities and opportunities in both tactile and visual intelligence applications[5], e.g., medical imaging, health monitoring as well as electronic skins[6]. Specifically, the tactile-enabled endoscope with transparent force feedback amounted onto its objective lens could detect and report potential physical contact with internal tissues and organs, and, as a result, it can serve as a desirable safety feature or navigation-guiding signals for clinical diagnostic and surgical operations of catheterization[7]. Furthermore, the highly transparent and sensitive tactile sensors can be introduced to wearable electronics, from which multiple physiological signals, such as arterial pressure waveforms, heart rates, respiratory rates, and blood pressure, can be detected in a continuous manner, while maintaining its optical imperceptibility[8]. In addition, the transparent human-machine interface could offer particular user experience by introducing 3D force sensing capacity into a conventional touch screen, allowing delicate object recognition and tactile feedback for augmented reality and gaming applications[9]. However, it remains challenging for current transparent flexible tactile sensors to achieve both ultrahigh level of optical transparency and device sensitivity in a single device.

Technically speaking, light transmittance reflects the overall level of light absorption and scattering in the medium as well as light reflection at the interface[10,11]. In order to improve the light transmittance of the tactile sensing device, current research mainly focuses on modifying intrinsic optical transparency of building materials. Although the optical loss due to absorption and scattering can be minimized by carefully selecting and modifying the material itself with the highest light transmittance of 99.94% reported[12], the overall transmittance of the device is still challenging to reach at a high level (e.g., greater than 95%), due to the light reflections presented at multiple material interfaces inside the sensor structure. Notably, the interfacial optical loss becomes considerably severe when coarse interfacial topology is encountered. Therefore, further improvement on device transparency demands on the alternative approaches to address the optical loss caused by such interfacial light reflections. For the tactile sensing devices to achieve a desirably high sensitivity, it is critical to engineer an interface with a high surface area for detection[13]. Therefore, multiple intriguing strategies have been further investigated, such as pyramidal, micro-needle, nanofibrous, and bioinspired structures, in order to create a 'coarse' configuration of the functional layer or the electrode[14]. Such interfacial topologies can lead to an improved device sensitivity as it generates a more appreciable level of deformation or a greater area of surface contact under the same external loads[15]. Unfortunately, these modifications may have adversely influenced the overall transparency of the device[16], which is mainly evaluated by light transmittance[5]. Therefore, the optical transparency of the tactile sensors, particularly that of the capacitive-based sensors,

[1]Department of Materials Science, Fudan University, Shanghai 200433, People's Republic of China. [2]Bionic Sensing and Intelligence Center (BSIC), Institute of Biomedical and Health Engineering, Shenzhen Institutes of Advanced Technology, Chinese Academy of Science, Shenzhen, Guangdong 518055, People's Republic of China. [3]Shenzhen Engineering Laboratory of Single-molecule Detection and Instrument Development, Shenzhen, Guangdong 518055, People's Republic of China. [4]C-MIND Center for MicroMedical Instruments and Devices, University of Science and Technology of China, Suzhou 215123, People's Republic of China. ✉email: yu.chang@siat.ac.cn; zgyang@fudan.edu.cn; tingrui@ustc.edu.cn

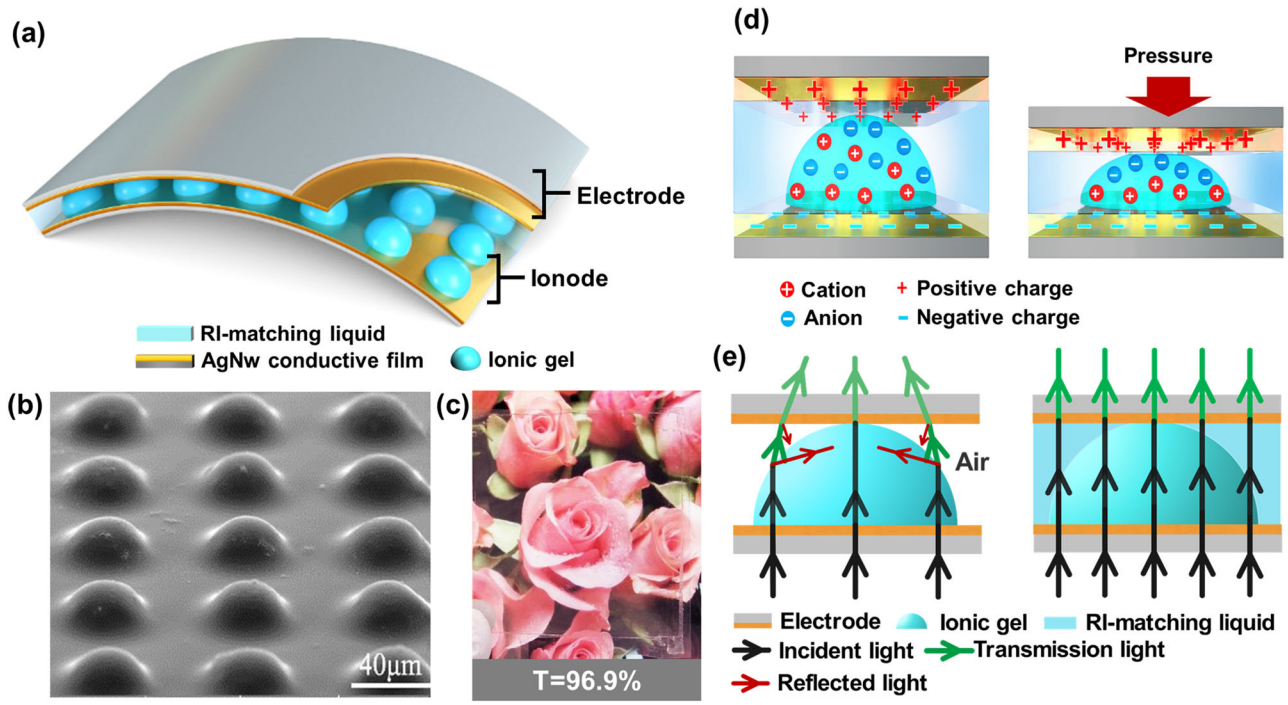

Fig. 1 TIS device illustration. a The structural illustration of the TIS device, **b** the SEM image of the ionic gel with build-in micro-hemispheric array, **c** a flower covered by the TIS device, representing an extremely high light transmittance of 96.9%, **d** the mechanical response mechanism of the TIS device, **e** the light paths of the TIS devices without and with RI-mating liquid filled.

has often demonstrated an inverse trend related to the device sensitivity[17].

Recent introduction of the flexible iontronic sensing mechanism (FITS) presents an approach to solve the standing issue in transparency improvement for tactile sensors, while offering ultrasensitive pressure detection, benefiting from its natural interface of ionic–electronic materials. Since its inception, the iontronic sensing has shown great potential in its characteristic advantage in optical transparency, as all the building materials can be intrinsically transparent, particularly the ionically functional materials. Meanwhile, it can possess an optically smooth interface of sensing[18]. Pan and his colleagues have built the first flexible iontronic pressure sensor with an optically clear structure, which contains a planar transparent ionic coating covering the bottom electrode separated from the top electrode by an air-filled spacing layer. However, the original iontronic sensor only demonstrates light transmittance of 77%, due to the optical loss at the air–solid interface[19]. Recently, Guo and his colleagues have reported a highly transparent iontronic sensing (TIS) material with a light transmittance of 94.8%, in which a porous Polyvinylidene Fluoride (PVDF) membrane has been infilled with an ionic liquid with matched refractive index (RI)[5]. However, the overall device light transmittance is only limited to 90.4%, as the optical loss between the ionic substances and the sensing electrodes in this architecture. Expectedly, the improvement on the optical transparency of the porous PVDF membrane decreases the coarseness at the interface, resulting in an undesired low sensitivity of about 1.2 kPa^{-1} as compared to the existing iontronic sensors. As a comparison, the state-of-art touch panel devices have already achieved a light transmittance of higher than 95% on the screen, since the current display applications requested the level of the device optical transmittance to be as high as possible for critical display brightness and clarity of the screen[20].

In this work, we have proposed a specific architecture of the TIS device, simultaneously enabling high device sensitivity, and fine optical transparency. By implementing a two-layer sensing architecture (as shown in Fig. 1a), the TIS device includes one transparent silver nanowire (AgNw) conductive film coated with an array of microscopic hemispherically shaped transparent ionic elastomer (Fig. 1b), referred to as ionode; and a pristine AgNw surface as the counter electrode. In between the ionode and the electrode, non-ionic RI-matching liquid, which can stably coexist with the gel for the huge difference on their hydrophilicity, has been filled to remove any reflective air–solid interfaces among the sensing structure. Remarkably, an outstanding level of optical transparency can be independently delivered in the TIS device without altering its sensitivity. Because the building materials are all intrinsically with high transparency, including the ionic sensing gel, the transparent electrodes as well as the RI-matching liquid, which present extremely low light absorption and scattering internally, yielding a high light transmittance at the material level. More importantly, the RI-matching liquid introduced to the sensing layer would significantly reduce the reflections at the interfaces, resulting in further improvement on the light transmittance of the sensor under the multiple-layer device architecture. As a result, an overall optical transmittance of 96.9% of the entire tactile sensor has been achieved, the highest reported value in literature to our knowledge (in Fig. 1c). On the other hand, a mathematic theoretical equation has been derived to quantitatively describe the mechanical response of the TIS device based on the elastic deformation of the micro-hemispheric array. Therefore, with both the optimal design of the micro-hemispheric microstructures and the intrinsically high sensitivity of the iontronic mechanism, the sensitivity of the device can reach at 83.9 kPa^{-1}, three orders of magnitude higher than that of the counterpart capacitive devices[1,5,17,21]. Benefiting from its comprehensive performance in sensing and optical characteristics, we have first demonstrated a TIS-integrated endoscope for both visual and tactile diagnostic functions, in which the transparent tactile sensing enables quantitative assessment of tissue stiffness in front of the optical element, while performing routine endoscopic imaging. Moreover, we have implemented invisible tactile reception in a wearable format, from which important hemodynamic parameters can be collected and analyzed in a real-

time and imperceptible manner. Furthermore, we have achieved transparent tactile imaging on top of an optical display with high spatial resolution for emerging human-machine interface. In consequence, the TIS devices hold enormous potential for the fast-evolving human-machine interfaces for industrial and medical applications, particularly where both high optical transparency and device sensitivity are demanded.

RESULTS

Operational principle

In order to achieve an ultrahigh transparent tactile sensor, optical and sensing analysis has been established to determine the critical parameters related to the transparency and sensitivity of the TIS device. In principle, the device transparency can be quantitatively evaluated by the light transmittance, defined as the ratio between intensities of the incident and the transmitting lights[10], which is specifically influenced by the reflection at the interface as well as the absorption and scattering within the medium[11]. The current optimization on the transparency would primarily focus on selecting the mediums with intrinsic properties of low absorption and scattering. Through the investigations on the compositions and structures for the material transparency, the state-of-art mediums, such as AgNw, ionic gel, graphene, PDMS, etc., have demonstrated extremely low adsorption and scattering in the transparent sensing structures. Notably, the transmittance loss from adsorption and scattering of the medium can only be of 0.1% level[22], which becomes almost negligible overall. In this study, therefore, we would confine our selection of structural materials from these established categories.

Besides the influences from the building materials, the interfaces between different layers contribute significantly to the transmittance loss caused by reflection. Importantly, the interface presented between the deformable sensing layer and the air gap in the sensing architecture could result in a significant light reflection, even in a planar surface, and this effect becomes further intensified with the interfacial irregularities[5]. In fact, the transmittance loss caused by light reflection at the interface has played a major role in determining device transparency, which has been with limited research in the existing transparent sensors due to their structural restrictions[23]. Specifically, the optical loss from the reflection at the interfaces can be described using the reflectivity R, which is defined as the intensity ratio between the reflected and incident lights, and can be quantitatively expressed as,

$$R = \left(\frac{n_2 - n_1}{n_2 + n_1}\right)^2 \quad (1)$$

where n_1 and n_2 represent the RIs of the mediums along the interface[10]. This equation is valid when the incident angle is zero, and it can be evolved into a more complicated format in a non-normal incident case (shown in supporting information). According to Eq. 1, the reflectivity is highly related to the RIs of the materials along the interface, and a smaller difference between RIs of the adjacent materials would lead to a lower reflectivity at the interface. Furthermore, the reflectivity can approach to a minimum (close to zero) if the RIs of the materials match with each other. This could also be true even the light incident angle is not 0°. In such a situation, most of light can penetrate through the interface at any incident angle without experiencing apparent transmission loss, even when the interface is rough, which implies the changes over the surface topology the adjustment on the surface morphology of the pressure sensitive interface would no long influence the device optical transparency. In the proposed TIS architecture, we have used all the building materials with high transparency and matched RI. Remarkably, we have introduced the RI-matching liquid to fill up the air gap between the electrode and the ionode, leading to considerable elimination of optical reflection at the ionode/air and air/electrode interfaces. Therefore, it can provide higher optical transparency than that of the existing counterparts in the device level.

To optimize the sensitivity of the TIS device, a mechanical model has been built, based on the fundamental principal of the iontronic mechanism, to determine the material properties and structural parameters of the TIS device. It is worth noting that the hemispherical microstructures have been chosen to establish the mechanical sensing topologies for the following reasons, first of all, the shape deformation of the hemispherical elastomeric structure has been well investigated, which can be theoretically defined in the classic mechanical model[24]. Secondly, the geometrical variables of the hemisphere can be easily adjusted to satisfy the desired sensing characteristics, such as sensitivity and resolution[13]. Furthermore, the hemispherical microstructure demonstrates superior stability and reliability over that of the alternative micropatterns containing sharp corners, such as pyramid microstructures under repetitive mechanical deformation, since its rounded shape relieves both the excessive stress concentration and the induced plastic deformation[13]. As external pressure P is loaded onto the electrode layer, it leads to elastic compressive deformation of the ionic microstructures of the ionode. As a result, the contact area between the electrode and ionode expands accordingly, along with the increment in the corresponding EDL capacitance, as expected in the iontronic sensing theory[19,25] (Fig. 1d). Particularly, the sensitivity S of the iontronic sensor within a small deformation limit can be described using the following equation derived from the classic Hertz contact model[24,26],

$$S = \frac{2kA \cdot \mathrm{UAC}}{3C_0} \cdot \left(\frac{\rho}{E}\right)^{\frac{2}{3}} \cdot \left(\frac{d}{P}\right)^{\frac{1}{3}} \quad (2)$$

Where C_0 stands for the initial iontronic capacitive readout without any load, and UAC represents the unit area capacitance between the ionic gel and electrode layers. ρ is the radius of curvature of the hemispheres, d refers to the density of the hemispherical array, and A denotes the sensing area. E and k indicate Young's modulus and Passion's ratio-related constant of the elastic gel material, respectively. The detailed derivation of Eq. 2 is illustrated in supporting information. As can be seen, the sensitivity of the device has positively correlated with the interfacial UAC, the sensing area, the radius of curvature, and the density of the hemispheric array, whereas Young's modulus of the gel and the initial capacitance exhibit inverse relationships with the sensitivity. In brief, for the sensitivity optimization, one could rely on designing the functional material and interfacial properties (E and UAC) as well as the geometrical parameters (ρ and d) of the hemispherical array for sensitivity improvement, while the transparency improvement focuses on both the intrinsic transmittance of the building materials and minimization of the light reflection at interfaces.

Optimization of material properties for TIS

According to the Operation Principle, several considerations need to be in place for the functional ionic gel material, including intrinsic transparency, elastic modulus, ionic concentrations as well as micro-processability. To this end, we have adopted a photo-crosslinkable polymeric gel approach containing active ionic contents to construct the sensing unit, since it meets the combined requirements of high optical clarity, high elasticity, tunable ionic contents, and direct photo-curability of the ionic gel material[3]. The ionic gel is composed of a hydrophilic ionic liquid 1-ethyl-3-methylimidazolium triflate (EMIMOTF) uniformly dispersed in a polymer matrix prepared from poly(ethylene glycol) diacrylate (PEGDA) and hydroxyethyl methacrylate (HEMA), as shown in Fig. 2a. EMIMOTF, a room temperature ionic liquid with a high conductivity of 8.858 mS/cm[27] and a high compatibility with

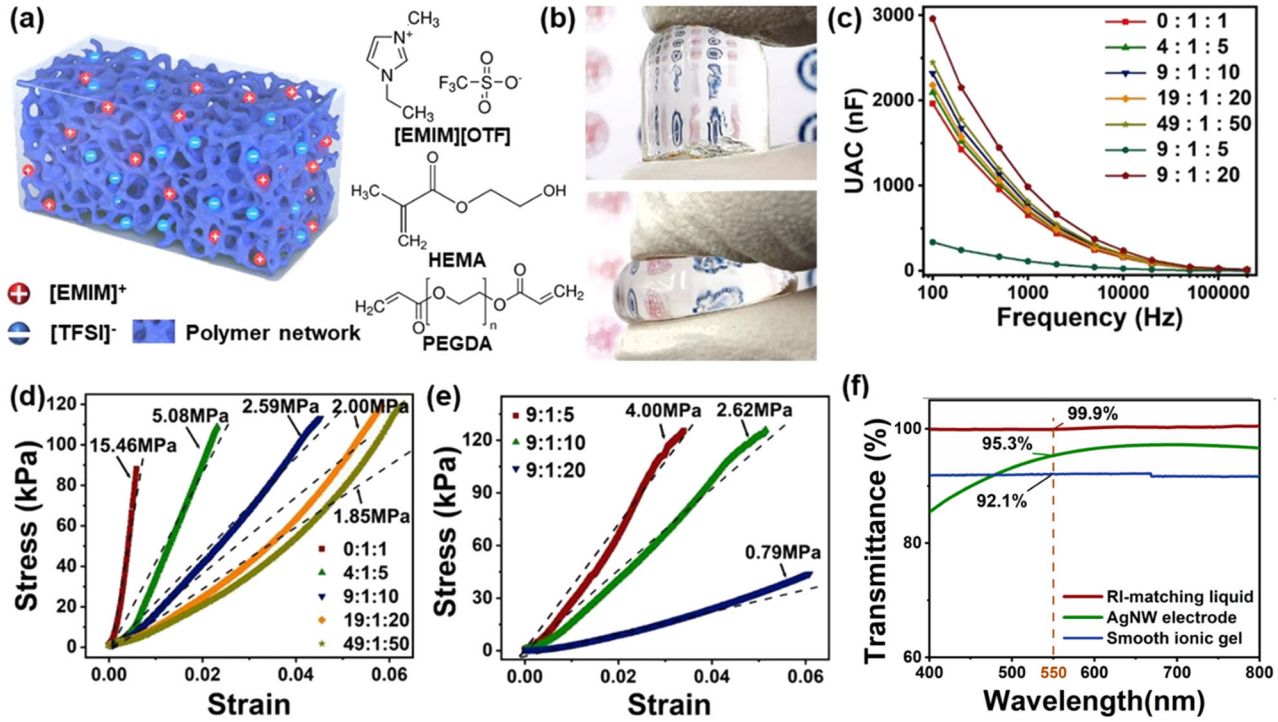

Fig. 2 The performance of the ionic gel for TIS device. a The molecular structure of the ionic gel, **b** the photos of the ionic gel indicating its high elasticity, **c** the UACs of the ionic gels with different compositions, **d** the Young's modulus of the ionic gels with different crosslinking densities, **e** the Young's modulus of the ionic gels with different ionic liquid concentrations. The inserted ratios in **c**–**e** are the weight ratio between HEMA, PEGDA, and [EMIm]OTf. **f** The visible spectrums of all the building materials of the TIS devices, which include the ionic gel, AgNw conductive film, and RI-matching liquid.

acrylate monomers, offers abundant mobile cation and anion for iontronic sensing. More importantly, EMIMOTF offers a much wider electrochemical window of 3.9 V compared to water[28], which can prevent the electrochemical reaction of AgNw under electric field, increasing the long-time stability and repeatability of the TIS device. PEGDA and HEMA can form a 3D molecular network through UV polymerization of acrylate groups, turning the liquid EMIMOFT into an ionic gel with high elasticity and deformability (Fig. 2b). The main selection criteria of HEMA is the hydroxyl group with high polarity, which can improve the compatibility between the polymer matrix with EMIMOTF[29]. Meanwhile, as a hydrophilic crosslinker, PEGDA is used to control the elasticity of the ionic gel. A higher concentration of PEGDA, which contains two acrylate groups, leads to a higher crosslinking density of the ionic gel. The reaction equation of the ionic gel is shown in Supplementary Fig. 3. This section will investigate and discuss influences on the relevant electrical, mechanical, and optical properties at the materials level, particularly, the ionic gel compositions to optimize the sensing responses as well as the intrinsic light transmittance of all the building materials to ensure the high optical transparency of the TIS devices.

As presented in Eq. 2, the sensitivity of the TIS device is linearly correlated to the UAC of the material interface, which can be fairly complicated and influenced by the material properties such as ionic species and concentrations, electrode materials, the environmental parameters, including temperature and humidity, and even the measurement techniques, such as driving frequency and potential, etc.[3,30,31]. In this work, the main approach to improve the interfacial UAC is to adjust the ionic concentration in the selected composite gel material under a controlled environment and established measurement condition. Figure 2c plots the interfacial UAC measurements using the ionic gels with different compositions from 20 Hz to 200 kHz at the voltage of 1 V, which is a widely used standard for the measurement of UAC[32]. It is expected that the interfacial UAC of the ionic gel decreases gradually with the rise of the driving frequency for the limited ion relaxation time, while a higher driving frequency leads to a higher sampling rate for capacitance detection, which is important for the response frequency of the device[25,30]. In order to achieve the balance between UAC and sampling rate, we will keep the electrical excitation and measurement at 1 kHz and 1 V for direct comparison. More importantly, by considering the ionic concentration in the gel matrix as a variable, a higher concentration of ionic contents would lead to a higher interfacial UAC. Particularly, the interfacial UAC with the material weight ratios among HEMA: PEGDA: EMIMOTF from 9:1:5, 9:1:10 to 9:1:20 (the corresponding ionic liquid concentrations of 33.3%%, 50%, to 66.7%) are measured at 112.3 nF, 766.9 nF and 985.4 nF, respectively. Further increments in ionic contents of the gel matrix would cause the exudation of ionic liquid even after curing, causing stability and reliability issues for the sensing material. Another finding is that if the ionic concentration is relatively stable, the crosslinking ratio has a very marginal influence over the interfacial UAC. For instance, a drastic change in the weight ratio between HEMA and PEGDA from 0:1 to 49:1 (the corresponding crosslinking ratios of 100–2%) leads to only about 25% increase in the interfacial UAC.

Another important material property related to the sensing performance of the TIS device is its Young's modulus according to theoretical analysis. In general, the modulus of the ionic gel can be controlled by adjusting the crosslinking density and the ionic liquid concentration in the gel. By adjusting the ratios among HEMA, PEGDA, and EMIMOTF from 0:1:1, 4:1:5, 9:1:10, 19:1:20 to 49:1:50, it forms polymer networks with different crosslinking densities of 100, 20, 10, 5, and 2%, respectively, and the relevant Young's modulus of the ionic gel can be altered from 15.46, 5.08, 2.59, 2.00 to 1.85 MPa, as summarized in Fig. 2d, since the polymer

chain movement is restricted with the increase of the crosslinking density. However, due to the low crosslinking density, the ionic gels with weight ratios of 19:1:20 and 49:1:50 demonstrate plastic deformation under pressure, leading to a poor recovery and repeatability of the tactile sensor. Moreover, changing the weight ratios between polymer monomer and ionic liquid can also control the Young's modulus of the ionic gel. A higher ionic liquid concentration can lead to a softer ionic gel matrix with a higher 'unrestricted volume' and lower interactions between polymer segments, as shown in Fig. 2e[33]. In this study, we have identified that the modulus as low as 0.79 MPa can be achieved when the weight ratio among HEMA, PEGDA, and EMIMOTF is set at 9:1:20. Unfortunately, this ratio would lead to exudation of the ionic liquid from the gel matrix under external pressure, affecting the stability of the device. Therefore, we would choose the weight ratio of 1:1 among curable monomer and ionic liquid as the primary parameters for the further investigation, given its relatively high elasticity (i.e., low Young's modulus) along with high stability.

As aforementioned, the high intrinsic light transmittances of all the building materials are the precondition of the high optical transparency of the TIS device. Figure 2f illustrates the visible spectrum of the ionic gel material (50 μm in thickness) with a ratio between HEMA, PEGDA, and EMIMOTF of 9:1:10, the AgNw conductive film, and the RI-matching liquid. As can be seen, the prepared smooth ionic gel shows a high light transmittance at the whole visible and near infrared spectrum, and a light transmittance of 92.1% compared with air is obtained at 550 nm, the standard wavelength for transparency comparison. It is worth noting that the intrinsic light transmittance of the ionic gel should be 99.5% as predicted in Supplementary Eq. 1, and the material absorption and scattering only contribute 0.5% transmittance loss ($e^{-(a+s)x} = 99.5\%$), since its molecular groups and the high structural uniformity possess low visible light absorption. The major loss on the light transmittance results from the light reflection at both interfaces against air. Moreover, the AgNw conductive film also has an extremely high light transmittance of 95.3% with an anti-reflection coating on its non-conductive surface, which can significantly reduce the light reflection at the solid-air interface[34]. Furthermore, RI-matching liquid is mainly composed of silicone oil and liquid paraffin, both of which present low absorption at the visible spectrum[35]. Therefore, the light transmittance of the RI-matching liquid in a cuvette with an optical length of 9.55 mm is measured to be 99.9% compared with a cuvette filled with deionized water. For a TIS device containing a RI-matching liquid layer about 25 μm in thickness, the light absorption and scattering of the liquid only cause negligible loss of 0.002% on transmittance accordingly. As a result, all the building materials used in the TIS device have been proven to possess high transparency according to both the literature and our experimental verifications.

The tactile sensing performance of the TIS device

The capacitance-to-pressure (*C–P*) performance is the key to the TIS device for it demonstrates several critical properties of the sensor including sensitivity, linearity, detection range, as well as anti-interference[6,8,30,36–39]. According to Eq. 2, the sensitivity of the TIS device with unit area confinement is related to the curvature radius of the hemisphere, and the density of the array. This section will discuss the influences of these parameters on the sensitivity of the TIS device, aiming to control and optimize the mechanical response of the sensor.

The geometrical parameters of the hemispheric array can be easily controlled through micro/nano manufacturing. As demonstrated in Eq. 2, a higher array density and a larger hemisphere lead to a higher sensitivity of the TIS device. Figure 3a plots the experimental investigations on the influence of the array density on the mechanical response curve of the TIS device. Different array densities of 27,778, 17,778, 10,000, and 4,444 cm^{-2} are achieved through UV curing of the ionic gels using the PDMS molds, corresponding to the hemisphere diameter/spacing of 50 μm/10 μm, 50 μm/25 μm, 50 μm/50 μm, and 50 μm/100 μm. Well matched with the theoretical predictions, the TIS device with an array density of 27,778 cm^{-2} (50 μm/10 μm) outputs the highest sensitivity of 83.9 kPa^{-1} in the pressure range of 0–20 kPa, considering the extremely low initial capacitance of 17.4 pF (shown in Supplementary Fig. 4). This value decreases to 20.4 kPa^{-1} from 20 to 100 kPa, agreeing well with theoretic prediction that sensitivity decreases with pressure advances. Figure 3b demonstrates the relationship between the hemisphere sizes and the pressure responses of the sensors. By keeping all the other variables unchanged (particularly, the array density), a larger hemisphere diameter leads to a higher device sensitivity of the TIS device. For instance, the sensitivity of the TIS sensor with a hemisphere diameter of 50 μm is 83.9 kPa^{-1}, which is 2.2 and 3.93 times of that with the hemisphere diameters of 20 and 10 μm. In practical, the hemispherical microarrary with the size greater than 50 μm should further improve the device sensitivity, however, it is difficult to prepare and maintain the consistency of such large hemisphere during the preparation of the mold through the reflow of the photoresist[40,41]. Since the maximal density of the hemispheres which can be achieved in given area is directly impacted by the unit feature size, we have also compared the *C–P* curves of the TIS devices with the maximal density of the hemispheres at various feature sizes, in particular, the hemisphere diameter/spacing of 50 μm/10 μm, 20 μm/10 μm and 10 μm/10 μm, respectively, as shown in Fig. 3c. the narrow spacing of smaller than 10 μm may lead to distorted patterns for the excessive depth-to-width ratio, especially the ones with a larger hemispherical size. According to Eq. 2, the diameter of the hemisphere plays a more influnence role on the sensitivity than that of the density. The measurement results have shown a good agreement with the model, in which the larger feature sizes would lead to a higher device sensitivty at the maximal array density, as expected. Specfiically, the sensitivitis can be calculated as 1:0.80:0.47, respectively, from the TIS sensors with hemisphere diameter/spacing of 50 μm/10 μm, 20 μm/10 μm, and 10 μm/10 μm. In order to verify the repeatability the TIS device, cyclic loads have been applied to the sensors. The results, summarized in Fig. 3d, indicate that nearly identical *C–P* response curve can be traced at a lower pressure level (<40 kPa), but a slight divation with a variable coefficient of 3% has been observed among a higher pressure range (from 40 to 100 kPa), which may be resulted from the system error of the loading device. Overall, the testing results have proven the high repeatability on the *C–P* response of the TIS device, as compared to the current tactile sensors, particularly, at a low pressure range[42]. In addition, the microscopic images of the ionic gels with different surface topologies have been illustrated in Fig. 3e. Considering the combined performance of the materials properties and geometrical parameters of the functional ionic gel array, it is determinted that the ionic gel with the weight ratio between HEMA, PEGDA and EMIMOTF of 9:1:10 and the hemisphere diameter/spacing of 50 μm/10 μm as the optimal selections for the construction of the following TIS devices.

Additional evaluations were carried out to evaluate the response time, repeatability, and resolution of the TIS device. The tests for the response rate were carried out using a piezoelectric actuator to apply a periodical load change (about 1 kPa) to the sensor, the results were summarized in Fig. 3f. Through the analysis of loading and unloading phases of each cycle, the response and reset times of the sensor, which was prepared using an ionic gel with optimized parameter, were measured at 61 and 50 ms, respectively. These values were not prominent compared with that of some classic iontronic

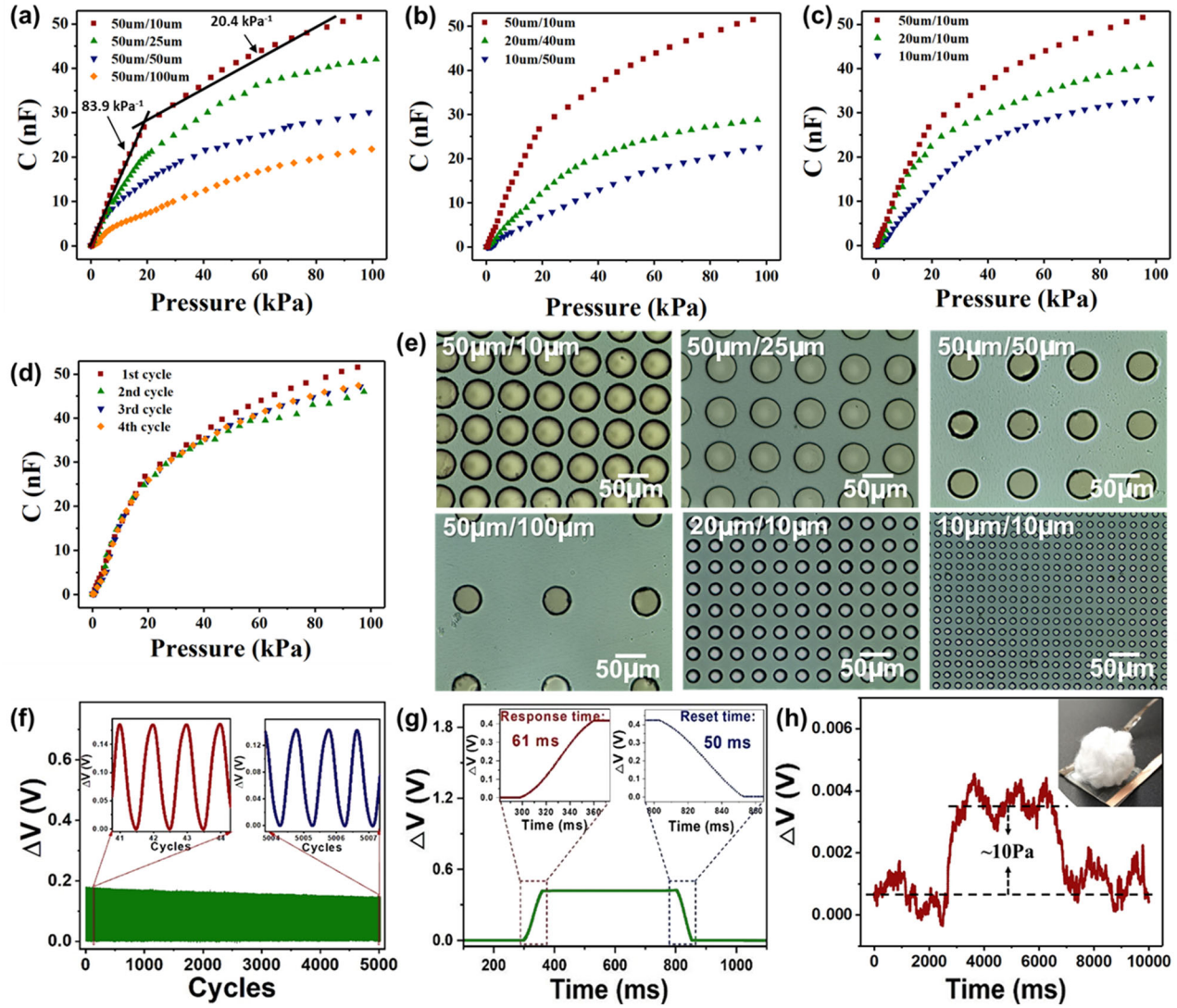

Fig. 3 The mechanical response of the TIS device. a The response (*C–P*) curves of the TIS devices using the ionic gels with different micro-hemispheric array densities, **b** the response (*C–P*) curves of the TIS devices using the ionic gels with different hemisphere diameters, **c** the response (*C–P*) curves of the TIS devices using the ionic gels with maximal density of the hemispheres at various feature sizes, **d** the repeatability of the response (*C–P*) curves of the TIS devices, **e** the microscopic images of the ionic gels with different surface topologies, **f** the characterization of the response and reset times in the dynamic loading test, **g** the repeatability test of 5000 cycles, and **h** the pressure resolution and detection threshold of the TIS device.

sensors, which could respond in sub-milliseconds, because the introduction of the RI-matching liquid extended the response time due to its high viscosity compared with air[42]. However, such response rates could have already satisfied a wide range of medical and industrial applications, such as measurement of arterial pulse wave and interactive human-machine interface[42]. Moreover, the repeatability of the tactile sensor was investigated under repetitive mechanical loads of 1 kPa at 5 Hz. Fig. 3g indicated that less than 10% variations in the signal magnitudes had been observed in the TIS device after 5000 duty cycles, proving its long-time stability and repeatability of the device. Finally, by taking the advantage of the noise-immunity of the iontronic sensing[3], the TIS devices have demonstrated a superior pressure resolution/ detection threshold of 10 Pa. Figure 3h exhibits that the real-time continuous recording from the TIS device by placing and removing an ultralight object (i.e., a cotton ball of 0.4 g) on the surface, proving the pressure resolution at 10 Pa.

Transparency performance of the TIS device

According to Eq. 1, the transparency of the TIS device is mainly determined by the absorption and scattering of all the materials and the reflections at all the interfaces. Ionic gel, as the key sensing material of the TIS device, has been experimentally measured at a low level (0.5%) of light absorption and scattering. As shown in Fig. 4a, the light transmittance of the smooth ionic gel is measured to be 92.1%, illustrating only marginal influence on the brightness and clarity of the image underneath. However, the ionode with the microarray configuration can cause significant light scattering, for instance, the one with the micro-hemispheric array of 50 μm/10 μm on diameter/space results in a low light transmittance of 35.4%. Because the surface irregularity substantially increases the incident angle of the light with a high level of reflectivity, as compared to the planar one, as shown in the photos in Fig. 4a. Inevitable, appreciable light reflection happens at the microstructured interface, leading to a degraded level of transparency in the TIS device.

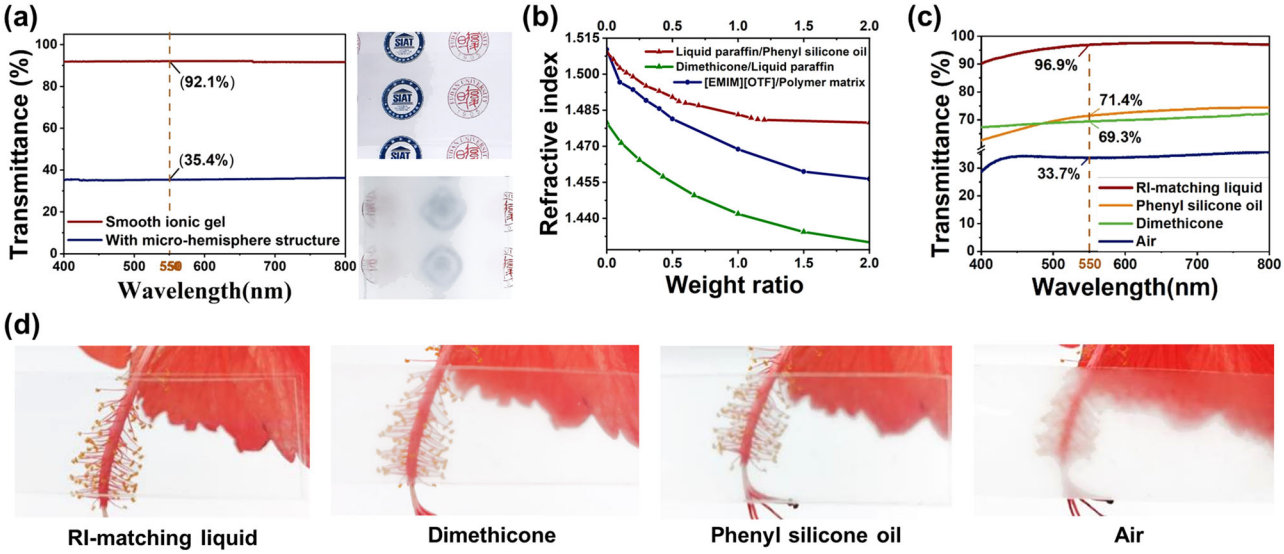

Fig. 4 The optical performance of the TIS device. a The visible spectrums of the ionic gel with and without surface micro-structure; **b** the RIs of the ionic gel and the RI-matching liquid with different components; **c** the visible spectrums of the TIS devices filled with the mediums with different RIs; **d** the comparison on the brightness and clarity of the images under the TIS devices using different mediums filled.

As aforementioned, the introduction of RI-matching liquid is to fill up the interfacial sensing gap between the electrode and the ionode, which can significantly reduce the light reflection at all the interfaces inside the device, particularly the one on the microarray side. Importantly, the RI-matching liquid needs to satisfy two main requirements: RI matching with that of the ionic gel and the chemical stability with the gel, which means it doesn't cause any material exchange of the ionic component or swelling of the gel matrix. The first requirement can be satisfied by preparing a mixture system containing both high and low RI components. Specifically, the mixing ratio between the two components can be used to adjust the RI of the RI-matching liquid. The other requirement can be solved by establishing an 'oil-water' antipathy system to achieve the stable coexistence between ionic gel and RI-matching liquid, of which the ionic gel is water-like hydrophilic, while the RI-matching liquid should be oil-like with high hydrophobicity. Such a hydrophobic-hydrophilic material interface shows eminent stability without apparent ionic liquid release or gel swelling[43]. In consideration of high hydrophobicity, high transparency, low evaporation, nontoxicity, and specific RI range, phenyl silicone oil (RI = 1.51), dimethicone (RI = 1.40), and liquid paraffin (RI = 1.48) have been selected for the RI-matching liquid as high, medium and low RI constituents respectively. The reason of adding a medium RI constituent is that phenyl silicone oil cannot mix with dimethicone to form a transparent liquid. Therefore, liquid paraffin is used to mix with phenyl silicone oil or dimethicone to form two bi-component systems with tunable RIs of 1.51–1.48 (phenyl silicone oil/liquid paraffin) and 1.48–1.40 (liquid paraffin/dimethicone) respectively, so that it can cover a wide range of RI matching, from 1.40 to 1.58, using the two-component system for different material constructs of the ionic gel, as shown in Fig. 4b.

To validate the performance of the RI matching strategy, we have compared the optical transparency of the TIS device before and after the introduction of the RI-matching liquid. As summarized in Fig. 4c, the TIS device with the air gap only demonstrates a light transmittance of 33.7%, significantly influencing the brightness and optical clarity of the image quality underneath the sensing surface. After filling the air gap using RI-matching liquids with different compositions, including pure dimethicone, pure phenyl silicone oil, and perfect matched composition of 1:10 between dimethicone and liquid paraffin, the results have suggested remarkable improvement on the light transmittance of the TIS device. Moreover, using an ideal RI-matching liquid ($\Delta n = 0$) to the ionic gel (RI = 1.4688) leads to the optimal performance of 96.9% in the transmittance measurement as compared to 69.3 and 71.4% when using dimethicone (RI=1.4030, $\Delta n = 0.0658$) and phenyl silicone oil (RI = 1.5110, $\Delta n = -0.0422$), which have greater RI differences with the ionic gel, respectively, in a good agreement with the theoretical predication. Fig. 4d illustrates the transparency variations of the samples using different matching mediums, among which the one using the ideal RI-matching liquid leads to the highest brightness and clarity of the image through the TIS device. As a result, an optical transparency of 96.9%, the highest in the literature to our knowledge, has been achieved through removing the air interfaces by the RI-matching liquid.

Performance comparison with current flexible transparent tactile sensors

Supplementary Fig. 6 along with Table 1 summarizes the performance comparisons of the TIS device with other flexible transparent pressure sensors in terms of both sensitivity and light transmittance. As aforementioned, the sensitivity and the light transmittance of the conventional flexible transparent sensor typically exhibit an opposite relationship; in another word, a higher sensitivity always leads to a lower light transmittance by comparing the literature, as shown in Supplementary Fig. 6[2,5,6,12,16,17,19,21,32,44–47]. It is mainly because the sensitivity improvement of the tactile sensor has been achieved by introducing coarse interfaces, which adversely cause additional light reflection at such interfaces. Alternatively, in this work, introducing the RI-matching liquid into the sensing layer provides a route to address the dilemma between high transparency and high sensitivity, by eliminating the light reflections occurring at the internal material interfaces. In summary, the proposed TIS device has used the elastic ionic gel matrix (with the weight ratios of HEMA, PEGDA, and EMIMTFSI at 9:1:10), which has high elasticity (with the Young's modulus of 2.59 MPa), ultrasensitive interface (with the high UAC of 766.9 nF), as well as high stability under pressure. The ionode is covered by the sensing layer of ionic gel structured into the hemispherical microarray configuration (with the diameter/spacing at 50 μm/10 μm). Additionally, the RI-matching liquid with that of the ionic gel matrix is introduced to

Table 1. The detailed performance specifications of the transparent pressure sensors cited in Supplementary Fig. 6.

Mechanism	Material	Sensitivity (kPa^{-1})	Transmittance	Ref. no.
Resistive	Graphene, PET, PDMS, and SU-8 spacers.	6.55	70.0%	2
Resistive	AgNWs, PET, PDMS	45.0	74.0%	6
Resistive	PDMS, KCl, Na2SO4	0.02	92.8%	12
Capacitive	PDMS, PEDOT: PSS	0.034	85.0%	16
Capacitive	PDMS, PEDOT: PSS	1.0	73.0%	17
Iontronic	ITO Film, iontronic film	1.0	77%	19
Iontronic	PVDF, ionic liquid, AgNw	1.2	90.4%	5
Capacitive	ITO, PDMS, PEDOT: PSS	0.025	82.0%	21
Capacitive	Pb(ZrxTi1-x)O3, ITO, PDMS	0.089	80%	32
Capacitive	PUA, PET, platinum, Ag nanoparticles	0.036	83.7%	44
Capacitive	AgNw, ITO, PDMS	0.831–0.5	71%	45
Resistive	Polyacrylonitrile, graphene	44.5	77.0%	50
Resistive	Poly acrylic acid, 1-ethyl-3-methylimidazolium dicyanamide	0.73	85.0%	46
Resistive	AgNw, UV curable polyurethane acrylate	10	85.0%	47
Iontronic	AgNw film, ionic gel, RI-matching liquid	83.9	96.9%	This work

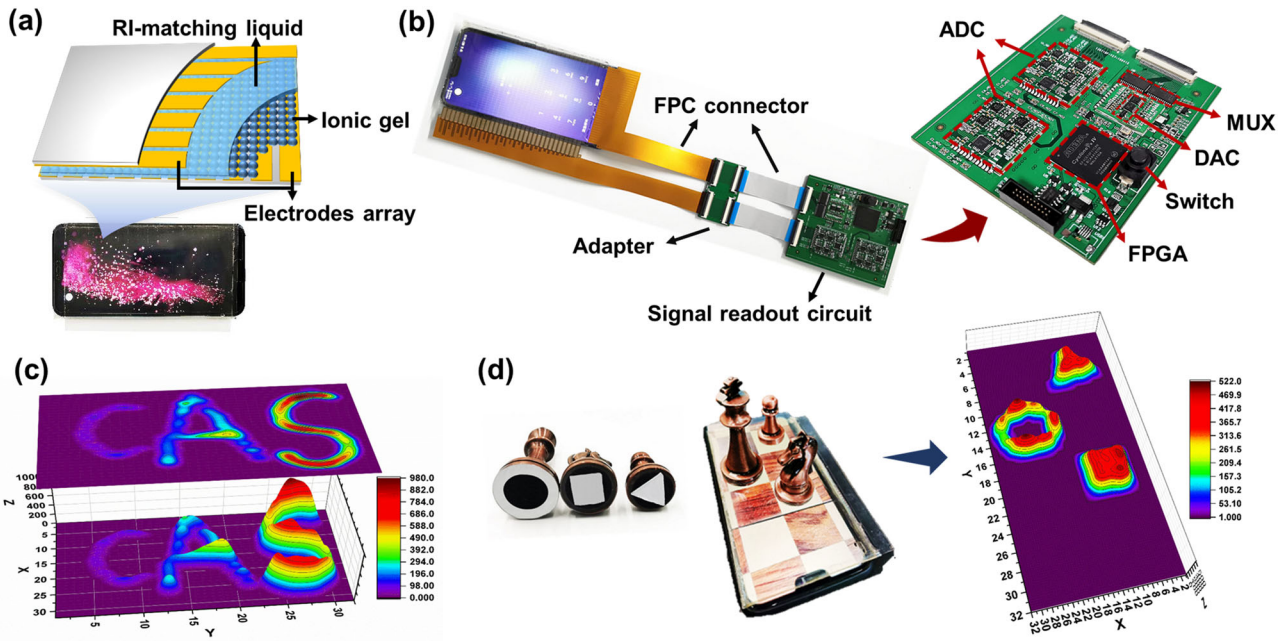

Fig. 5 The demonstration of transparent tactile AI. a The TIS touchscreen with a 32 × 32 sensing array attached on the screen, and the structural schematic diagram of the TIS array, **b** the TIS touchscreen system and the design of the signal readout circuit **c** the captured pressure heat map when writing "CAS" with a finger on the screen, **d** a typical application scenarios of object recognition using TIS touchscreen: virtual chess game on a displaying device using real pieces.

the sensing layer to remove all the reflective air–solid interfaces. As a result, the TIS device exhibits superior performance overall (i.e., the sensitivity of 83.9 kPa^{-1} and the light transmittance of 96.9%), which are highest in the literature, among the existing flexible transparent tactile sensors.

Transparent tactile AI: transparent 3D touchscreen for human-machine interface

Given its distinct high transparency and high sensitivity, the TIS device can be prepared to adhere onto any screen or display, turning it into a pressure-sensitive touchscreen device, referred to as TIS touchscreen. The conventional 3D touch devices, which is pressure-sensitive but not optically transparent, can only be amounted at the backside of the optical display, further reducing its device sensitivity and spatial resolution. On contrast, the TIS touchscreen with the extremely high transparency can pass the high-brightness and high-clarity contents on the display with a minimal optical loss (less than 4%), while maintaining its high device sensitivity and enabling detection of delicate objects and tactile feedback for augmented reality. Therefore, the TIS device can be simply amounted on top of any existing non-touch sensitivity display and simultaneously upgrade it to a pressure-sensitive instrument. Figure 5a illustrates that the TIS touchscreen with 32 × 32 sensing units has been implemented by patterning the top electrode and the bottom ionode into an orthogonal scanning array with a spatial resolution of 2 × 4 mm^2. The high-

resolution pressure sensing matrix can be of particular interest as an interactive input method during pressing, writing, or drawing, offering the pressure/force value on the third axis besides only the positioning information on the *X*–*Y* planes. Figure 5b illustrates the circuit system of the TIS touchscreen. The row and column electrodes array in the TIS touchscreen are bonded with two FPC connectors via anisotropic conductive adhesive (ACF) respectively, then connected with the signal readout circuit. The readout circuitry mainly composed of row selection unit (MUX), data acquisition unit (ADC), decode unit (DAC), and control unit (FPGA). A programmed FPGA output a control signal to select different rows in the matrix by the MUX, and the signals of all the units of the selected row will be amplified through an op-amp and acquired by the ADC, after the signals processing by FPGA and signals decoding by DAC, the collected information of all the rows will be transmit to Labview for recording and displaying, as shown in Supplementary Fig. 7. Figure 5c demonstrates the captured pressure heat map of 'CAS' by finger touch with different contact pressures (gentle, mild, and strong) among distinct letters in a high-definition fashion on the TIS touchscreen. Such a heat map traces the pressure variations of each individual sensing element in real time during writing, which can be further used to differentiate the writing patterns or signatures from different people as a biometric identification method for encryption applications in HMI[36,48]. Furthermore, with heat map of contact pressure information in the TIS touchscreen, one can develop an object-recognition algorithm to identify different objects for tactile-enabled artificial intelligence[9]. In particular, the physical contact between any object and the display would form a static pattern of pressure distribution, of which the heat map contains both the shape and weight information for further AI analysis. By extending the power of such tactile AI, one can convert a virtual chess game into a real one, of which the chess pieces stand on the TIS touchscreen for playing. In this scenario, chess pieces are configured with various shapes of contact at its bottom, and the corresponding heat maps of the pressure distribution contains distinctive key features of each piece, so the touchscreen can read the pieces and the movements by their contact heat map information as shown in Fig. 5d. As a result, the TIS touchscreen has shown great potential on the next-generation human-machine interface for input, identification, as well as augmented reality applications.

Medicine tactile AI: Integrated endoscopic optics with TIS tactile sensing

Another important application for transparent tactile sensing is within the fast-growing field of clinical endoscopic imaging and surgeries, where a small-sized optical element in a catheter or tube format is inserted into a human natural cavity, most commonly into the gastrointestinal tracks[49,50]. Theoretically, the endoscope with tactile sensing function can integrate the contact force information with visual image, which is highly potential for the purposes of tactile feedback and tissue stiffness measurement during routine endoscopic inspection[51].

In order to provide tactile feedback for clinical safety as well as navigation purpose, current research has been mainly focused on the integration of the classic MEMS force sensors with solid structural build onto the endoscope head[7]. Because these MEMS devices are not transparent but rigid, these approaches always lead to rather complicated mechanical designs to adapt the solid-state sensors to the limited space on the endoscopic instrument, resulting in considerably high equipment cost as well as reduced system reliability. Even though, the direct contact with the optical lens cannot be easily detected through such a complex device architecture. In this work, we have upgraded the traditional MEMS sensors with the TIS device for the endoscopic tactile feedback. Unlike the complicated structural design to transmit the contact force, the highly transparent and ultra-flexible TIS device can be directly amounted onto the surface of the optical lens of the endoscope, without noticeable compromise of its optical performance. Figure 6a, b has illustrated the assembly and the integrated versions of the TIS device onto the endoscopic head with LED illumination surrounded, respectively. Specifically, the head size of the endoscope has been limited to 3.7 mm in diameter to navigate through natural cavities. Accordingly, a TIS device with the same diameter has been prepared and perfectly integrated onto the endoscope within the head size. In addition, we have modified the electrical packaging of the TIS device by connecting the flexible electrodes inside the endoscope, which prevents the exposure of the electrical connections from the liquid surrounding during endoscopic procedure. As a result, such a miniature TIS device has been successfully integrated with the endoscope to enable the tactile functions in the optical system with a marginal influence on the brightness and clarity of the images obtained (in Supplementary Fig. 8). Furthermore, we have applied the TIS-enabled endoscope to navigate through a pancreas model with real pancreatic and pancreatic cancer tissues placed inside, mimicking the in vivo situation (Fig. 6c). Once a direct contact occurs between optical lens and the tissues, the capacitive readout of the TIS device would show a substantial increase, which can be converted into a force scale for the safety consideration. Figure 6d illustrates the contact pressure measurements from repetitive touches of the TIS-enabled optical head on the model. As can be seen, gentle touch forces as small as 1 mN can be easily resolved in the sensitive tactile feedback, which can potentially prevent the surgical damage or provide the delicate surface information for robotic navigation.

The endoscope system integrated with transparent electronics can also provide physical, chemical, and biological information about the tissue, which can facilitate the characterization and removal of tumors during endoscopic inspection. Previous research has provided impedance-based sensing, pH-based sensing, contact sensing, and temperature mapping, in combination with RF ablation therapy of the tumor tissue[52]. Here, another important parameter, tissue stiffness, can be obtained through the endoscopic tactile measurement. Tissue stiffness reflects the tissue composition and heterogeneity, which are often altered during the disease progression[53]. For instance, malignant tumors are generally harder than the normal tissue and the benign tumors[54]. Therefore, the integrated tactile measurement of the tissue stiffness could provide a facile method to endoscopically screen malignant tumors in real-time, while visual inspection cannot resolve such information in situ[55]. In order to establish a quantitative assessment of the tissue stiffness, the following procedure has been implemented. Firstly, the endoscope is applied to the sample in a constant speed until a certain safety limit has been reached. Subsequently, the slope rate of the curve (S) between the displacements of the endoscope and force outputs of the TIS device has been calculated. In the classic biomechanical theory, the stiffness, represented as Young's modulus (E), of the sample has an empirical relationship with the slope rate, as follows,

$$\lg E = \frac{a}{S} + b \tag{3}$$

where a and b are constant, implying that the sample with a greater value of S corresponds a higher material stiffness from the test[56]. This can lead to quantitative assessment of tissue properties by the TIS-enabled endoscopic system. For instance, the stiffnesses of the pancreatic cancer (Fig. 6e) and the normal pancreatic tissues (Fig. 6f), of which the former has a considerably higher stiffness than that of the latter one due to the severe fibrosis, have been measured and compared. Three calibration samples, i.e., PDMS ($E = 1.03$ MPa), Ecoflex ($E = 0.07$ MPa), and the 1:1 mixture ($E = 0.37$ MPa), with the known Young's moduli have

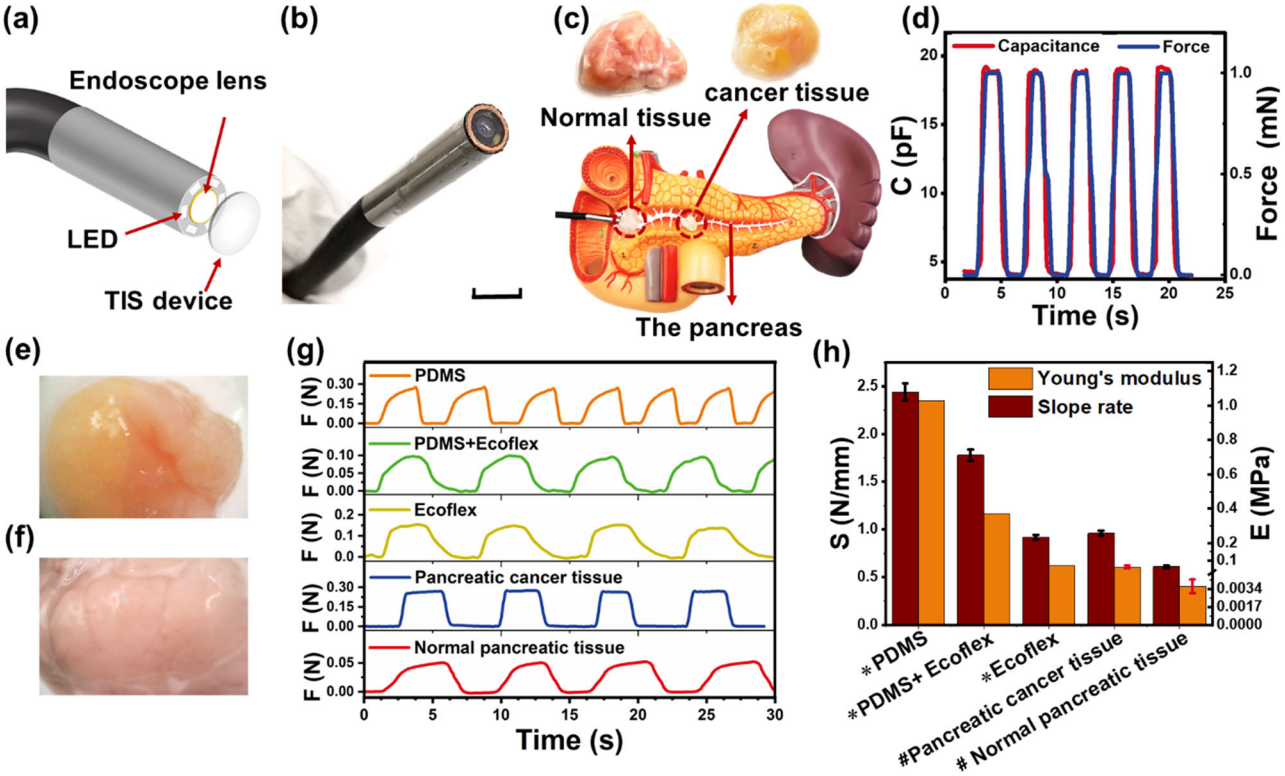

Fig. 6 The demonstration of medicine tactile AI. a The diagram of the TIS device attached on the endoscope lens, **b** the photos of the TIS-enabled endoscope, **c** the endoscopic inspection of the TIS-enabled endoscope in a pancreas model, and **d** the detected tiny force of the contact with the tissue, **e** the pancreatic cancer tissue and **f** the normal pancreatic tissue used for stiffness measurement, **g** the raw data for stiffness measurement of PDMS, PDMS/Ecoflex mixture, Ecoflex, pancreatic cancer tissue and normal pancreatic tissue, **h** the measured slope rates and the calculated Young's modulus (the '*' marks the referenced values from standard tensile test and the '#' marks the calculated values from Eq. 3) of different samples for stiffness test.

been pre-examined to determine the constants (a and b) in Eq. 3. The Young's moduli of the calibration samples are obtained from their strain-stress curves, which are shown in Supplementary Fig. 9. Figure 6g has summarized the stiffness measurement data of four cycles from all real and calibration samples, while the visual inspection from the endoscope over those samples has been conducted simultaneously without any interference. Through the analysis of the measurement data, the slope rates S (N/mm) of all the samples are obtained as 2.44 ± 0.088 for PDMS, 1.78 ± 0.058 for PDMS/Ecoflex mixture, 0.92 ± 0.024 for Ecoflex, 0.96 ± 0.027 for pancreatic cancer tissue, and 0.61 ± 0.014 for normal pancreatic tissue, as shown in Fig. 6h. As a result, Eq. 3 can be fitted with $a = -2.065$ and $b = 0.943$, from which the stiffnesses of the normal pancreatic tissue and the pancreatic cancer can further be calculated as 3.662 ± 0.648 and 62.37 ± 8.64 kPa, respectively. Both of stiffness measurements are within the reported ranges by other means from the literatures, and more importantly, the diseased tissue exhibits a significantly higher value than that of the normal one expectedly[57,58]. In brief, the TIS-enabled endoscope, combining visual and mechanical measurement capacities, can quantitatively substantiate the differences between the stiffnesses of the normal and malignant tissues, along with the optical observation, offering a potential direction for multifunctional endoscopic diagnosis in future.

Invisible tactile AI: Wearable TIS device for imperceptible health monitoring

In additional to performing measurement of contact pressure on various optical devices, the TIS device can also be configured into a wearable and imperceptible format for real-time monitoring of arterial pulse waveforms. The pulse waveform measurements can be achieved by applying a gentle pressure onto the sensing area through a finger or a wristband[59]. Figure 7a, b have demonstrated a circular shaped TIS device with a diameter of 2 cm can be directly attached to human skin, in order to acquire biomechanical signals from the arterial blood pulses or muscular movements, almost in an invisible manner due to its high optical transparency. When it is amounted onto the temple and wrist regions, the repetitive arterial pulse waveforms can be detected in high fidelity, which can be converted to about 75 and 65 beats min^{-1} of the volunteers, respectively. Given its high sensitivity, the detected signals can further reveal all the important features of the pulse waveforms in detail, including the systolic peak (P_1), reflected systolic peak (P_2), dicrotic peak (P_3) and end-diastolic pressure (P_4). These characteristic peaks can be used to quantitatively evaluate the pertinent hemodynamic parameters in real time, including arterial augmentation index, which are closely related to the arterial stiffness and blood pressure, etc.[60]. Therefore, early cardiovascular events or symptoms may be predicted through big data analysis from such continuously collected data sets. Unlike other alternative devices, the high transparency of the TIS sensor offers the patients with comfortable health monitoring capacity through the flexible yet unnoticeable wearable device, still yielding high-fidelity high-resolution signals, in consideration of patient privacy[42].

DISCUSSION

In summary, a flexible transparent tactile sensing device based on the emerging iontronic sensing mechanism has been developed

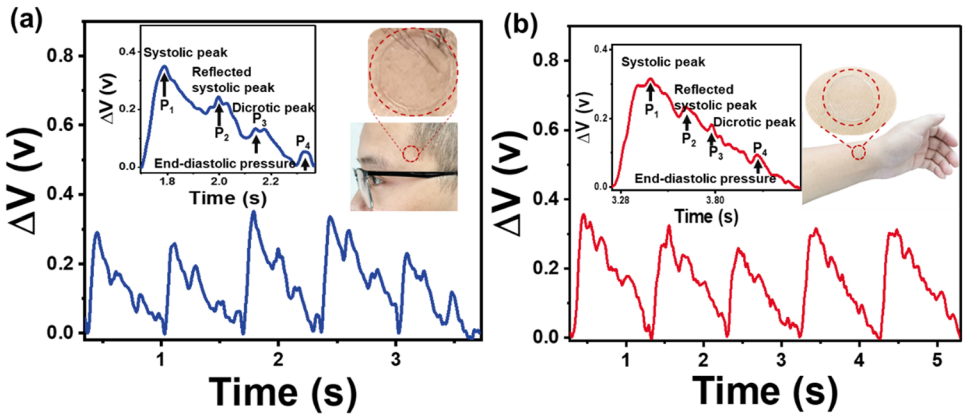

Fig. 7 The demonstration of invisible tactile AI. a The pulse wave signal collected by the TIS device at temple, the inserted image illustrates the detailed waveform of single pules wave, **b** the pulse wave signal collected by the TIS device at wrist, the inserted image illustrates the detailed waveform of single pules wave.

with combined features of ultrahigh optical transparency and high sensitivity. The flexible sensing structure is composed of a simple two-layer structure, i.e., an ionode layer covered by a micro-hemispherical ionic gel array and a transparent electrode layer to form the sensing structure, both intrinsically highly transparent to eliminate internal light adsorption and scattering, while a RI-matching liquid with the same RI of the ionic gel is filled into the space between the two layers to remove any highly reflective air–solid interfaces. It is worth mentioning that the highly hydrophobic RI-matching liquid can stably coexist with the hydrophilic ionic gel through the 'oil-water' antipathy principal. With such a RI-matching strategy, it could significantly reduce the reflections at all the interfaces inside the TIS device, improving the light transmittance of the sensor to 96.9%, which is the highest reported value in literature to our knowledge. In addition, a theoretical mechanical model has been derived to provide a quantitative relationship between the pressure and the output of the TIS device using the elastic deformation of the micro-hemispheric array. Remarkably, the device sensitivity can be optimized to 89.4 kPa^{-1} through the control of the electrical and mechanical properties of the functional materials, as well as the adjustment of the geometrical parameters of the micro-hemispheric array (e.g., its sizes and array densities), which is three orders of magnitude higher than that of the conventional counterpart capacitive devices. By using the RI-matching strategy, such modification on the surface micro-structure of the functional interface will not influence the optical transparency of the device, achieving both the ultrahigh transparency and device sensitivity in the single device structure. Overall, the reported TIS device has extended the optical transparency to the optimal level based on the feature of the intrinsically transparent device architecture and the RI-matching strategy, while the superior device sensitivity can be achieved simultaneously without affecting the optical transparency of the device by the iontronic sensing principle. Benefiting from such combined advantages, the TIS device has shown enormous potential in the emerging medical and industrial applications, including human-machine interfaces, medical and health monitoring, where high sensitivity and high transparency are both required.

METHODS

Preparation of ionic gel

Mixed designed amount of HEMA (96%, Hydroxyethyl methacrylate, Aladdin Reagent Company), PEGDA(Average Mn 400, Poly(ethylene glycol) diacrylate, Aladdin Reagent Company), and EMIMOTF (98%, 1-Ethyl-3-methylimidazolium trifluoromethanesulfonate, Aladdin Reagent Company) in a glass beaker, then added 0.5% wt silane coupling agent (97%, 3-(Trimethoxysilyl) propyl methacrylate, Aladdin Reagent Company) for adhesion improvement with the substrate and 5%wt photoinitiator (97%, 2-Hydroxy-2-Methyl-1-phenyl-1-Porpanone, Aladdin Reagent Company) to initial the polymerization. After that, the mixture was magnetically stirred at 400 rpm for 30 min to obtain a uniform precursor. Finally, dropped the mixture into a mold and covered it with PET film to isolate it from oxygen, followed by UV exposure at 365 nm for 30 s to form the ionic gel with the shape of the mold.

Preparation of PDMS mold

The micro-hemispheric array configuration was prepared based on the reflow of photoresist according to literature reports[40]. A foam tape with a thickness of 2 mm was adhered on the frame of the photoresist template prepared on glass. Then a mixture of 184 silicone rubber (SYLGARD™ 184 Silicone Elastomer, Dow Chemical Company) and curing agent (SYLGARD™ 184 Silicone Elastomer Curing agent, Dow Chemical Company) at a mass ratio of 10:1 after stirring and vacuum de-foaming was poured onto the template, and cured in an oven at 100 °C for 35 min to obtain a PDMS mold with hemispherical pits array configuration. The entire process to prepare the PDMS mold is shown in Supplementary Fig. 10.

Preparation of transparent electrode

As shown in Supplementary Fig. 11, An anti-reflection (AR) PET film (50 μm in thickness, Shenzhen Shenyu Technology Co., Ltd) with a light transmittance of 98% was used as the transparent substrate. AgNw ink (SNW-0501, Guangdong Nanhai ETEB Technology Co., Ltd) was coated on the AR PET film using a Mayer bar to form a wet film of 10 μm in thickness. After drying in an oven at 120 °C for 30 min, the transparent AgNw electrode was prepared.

Preparation of single point TIS device

First, the transparent bottom electrode was cut into the required shape by a laser cutter (JG15S-SP-12v, ZhengYe technology). Afterwards, dropped the ionic precursor mixture on the bottom electrode, and then covered it with the PDMS mold slowly from one side to another. Then a squeegee was used to gently remove any appreciable bubbles trapped in between. The precursor mixture was then UV cured (GGJ-ST-3000, Ling Wei) for 30 s. After uncovering the PDMS mold, an ionic gel with a hemispherical array configuration was prepared on the bottom electrode. Next, a frame of double-sided adhesive (Nitto 5600 of 5 μm in thickness, Nitto 5601 of 10 μm in thickness and Nitto 5603 of 30 μm in thickness) with the same thickness of the hemisphere radius was pasted on the ionic gel to bond the edges of the top electrodes firmly. Finally, the RI-matching liquid with a RI equal to that of the ionic gel was injected between the top electrode and the ionic gel to expel all the air (placed into a vacuum chamber to expel all noticeable air bubbles) and thus forming the TIS device after sealing the needle port using epoxy adhesive. The entire process to prepare the single point TIS device is shown in Supplementary Fig. 12.

Capacitance-to-pressure performance test

A single point TIS device with an area of $3 \times 3\ cm^2$ was fixed on a moving stage (KMTS50E/M, Thorlabs) and moved at a speed of 0.2 mm/min to a dynamometer (M5–10, Mark-10). A silicone rubber pad of $1 \times 1\ cm^2$ was set on the top the dynamometer head to apply uniform pressure to the central area of the TIS device. An LCR meter (TH2829C, TongHui) was used to measure the capacitance of the device with a driving frequency of 1 kHz and a peak-to-peak voltage of 1 V. The capacitance-to-pressure performance of the TIS device was tested by recording the force measured by the dynamometer and the capacitance value measured by the LCR meter simultaneously.

Initial capacitance measurement

The capacitance of the TIS device for capacitance-to-pressure performance test was measured for 20 s using an LCR meter (TH2829C, TongHui). The average capacitance during 3 cycles was treated as the initial capacitance of the TIS device.

UAC test

The prepared $1 \times 1\ cm^2$ ionic gel with smooth surface was sandwiched between two electrodes. A translation stage was used to apply about 100 kPa pressure to the structure to ensure a complete contact between the electrodes and the ionic gel. An LCR meter was then used to measure the capacitance of the structure through two electrodes with a sine signal from 100 to 20,0000 Hz and a peak-to-peak voltage of 1 V.

Young's modulus test

Prepared the ionic gel into a cylinder with a diameter of 30 mm and a height of 20 mm. The cylinder was placed on the bottom of a single-column force tester (ESM303, Mark-10 Corporation), and compressed at a speed of 13 mm/min. A dynamometer (M5–200, Mark-10 Corporation) was used to record the force applied to the cylinder. The engineering stress strain curve of the ionic gel was then plotted according to the strain calculated from the measured displacement, and the stress calculated from the measured force. The Young's modulus of the ionic gel was thus obtained from the slope of the curve at relatively low strain range.

Light transmittance test

The light transmittance was measured by an ultraviolet-visible spectrophotometer (Lambda 25, PerkinElmer) from 400 to 800 nm. The light transmittances of all the samples were compared with air except RI-matching liquid, which was compared with deionized water.

Response rate test

Response rate of the sensor was conducted via driving a piezoelectric beam (QDTE52–1, PANT) with a square wave (signal frequency is 1 Hz, peak to peak voltage is 20 V) generated by signal generator (AFG1022, Tektronix) to apply a 1 Hz periodic contact pressure about 1 kPa (measured via a dynamometer) to a single point TIS device of $1 \times 1\ cm^2$, and the real-time capacitance curve of the device was recorded by a data acquisition card (DAQ, NI USB-6361, NI Instruments Corporation). The system setup of the response rate test is shown in Supplementary Fig. 13, and the signal readout circuit for single point TIS device is shown in Supplementary Fig. 14.

Repeatability test

The process of the repeatability test is the same with that of the response rate test. The only difference is that the signal frequency is 5 Hz for repeatability test.

Transparent tactile AI: transparent 3D touchscreen for human-machine interface

Preparation of TIS screen system. The 32×32 TIS array was made following the same process with the preparation of the single point TIS device, except for the electrodes preparation. Here, UV laser was used to cut the AgNW coating on the top and bottom electrodes to form the strip pattern, and the patterns were orthogonally aligned before the bonding of the top electrode. The TIS array was then connected with the signal readout circuitry using an FPC connecter through anisotropic conductive film (ACF, 50 μm in thickness, 3 M 9703) bonding process.

Medicine tactile AI: Integrated endoscopic optics with TIS tactile sensing

Preparation of TIS device integrated on endoscopic optics. First, all the elements were prepared into designed shapes by laser cutting, of which the transparent electrode was a circles of 3.7 mm in diameter, ACF and double-sided adhesive (Nitto 5601) were circular rings of 0.3 mm in width, and flexible copper coated polyimide film (CPF, prepared by spraying 1 μm copper layer on 25 μm polyimide film) was a circular ring with a tail for connecting the readout circuit. Afterwards, all the elements were assembled into the TIS device with a layered structure of bottom transparent electrode, ACF, flexible CPF, double-sided adhesive, flexible CPF, ACF, and top transparent electrode, of which ACF was used to bond transparent electrodes and CPF. Before covering the top electrode, the pre-prepared ionic gel with a micro-hemispheric array structure on top surface was placed on the bottom electrode, followed by injecting RI-matching liquid. Finally, after covering the top electrode, the TIS device was integrated on the top of an endoscope using optically clear adhesive (K-3022, Kafuter). The entire preparation process is shown in Supplementary Fig. 16.

Test setup for endoscopic inspection with tactile sensing. The TIS device integrated endoscope was fixed on a moving stage (KMTS50E/M, Thorlabs) and moves towards the samples (pancreas model or different tissues on a platform) at a velocity of 1 mm/min. The signals of the TIS device during the entire process was recorded by the readout circuit for single point TIS device shown in Supplementary Fig. 14, and displayed by Labview software in real-time. In the readout circuit, a signal generator (AFG1022, Tektronix) output a sinusoidal signal (1 kHz and 1 V in peak-to-peak value) to the TIS device, followed by amplifying this signal using an operational amplifier with adjustable feedback resistor, and finally read by the DAQ. The photos of the test setup for endoscopic inspection with tactile sensing were shown in Supplementary Fig. 17.

Human tissue information. Pancreatic ductal carcinoma sample was obtained from pancreatic head of patient who underwent pancreatic cancer surgery at the Shenzhen Second People's Hospital of China. The non-occupational patient without disease history was recruited with consent in this study and handled in accordance with approved protocols from Institutional Review Board of the Shenzhen Second People's Hospital and Shenzhen Institutes of Advanced Technology, Chinese Academy of Sciences (SIAT-YSB-2021-Y0213).

Invisible tactile AI: Wearable TIS device for imperceptible health monitoring

The TIS device for health monitoring with a diameter of 1 cm was prepared following the process pf preparation of single point TIS device. After sticking on the skin using double-sided adhesive (Nitto 5603), the signals of the TIS device was recorded using the readout circuitry for single point TIS device.

Bio ethics statement. Pancreatic ductal carcinoma sample was obtained from pancreatic head of patient who underwent pancreatic cancer surgery at the Shenzhen Second People's Hospital of China. The non-occupational patient without disease history was recruited with consent in this study and handled in accordance with approved protocols from Institutional Review Board of the Shenzhen Second People's Hospital and Shenzhen Institutes of Advanced Technology, Chinese Academy of Sciences (SIAT-YSB-2021-Y0213).

DATA AVAILABILITY

The data that support the findings of this study are available from the authors on reasonable request. The authors declare that the data supporting the findings of this study are available within the article and the corresponding Supplementary Material File.

CODE AVAILABILITY

The code that supports the results within this paper and the other findings of this study are available from the corresponding authors upon reasonable request.

Received: 2 November 2021; Accepted: 30 March 2022;
Published online: 30 June 2022

REFERENCES

1. Guo, H. et al. Highly stretchable and transparent dielectric gels for high sensitivity tactile sensors. *Smart Mater. Struct.* **28**, 24003 (2019).
2. Pyo, S., Choi, J. & Kim, J. Flexible, transparent, sensitive, and crosstalk-free capacitive tactile sensor array based on graphene electrodes and air dielectric. *Adv. Electron. Mater.* **4**, 1700427 (2018).
3. Chang, Y. et al. First decade of interfacial iontronic sensing: From droplet sensors to artificial skins. *Adv. Mater.* **33**, 2003464 (2021).
4. Wu, Y. et al. A skin-inspired tactile sensor for smart prosthetics. *Sci. Robot.* **3**, eaat0429 (2018).
5. Liu, Q. et al. Highly transparent and flexible iontronic pressure sensors based on an opaque to transparent transition. *Adv. Sci.* **7**, 2000348 (2020).
6. Jo, H. S. et al. Wearable, stretchable, transparent all-in-one soft sensor formed from supersonically sprayed silver nanowires. *ACS Appl. Mater. Inter.* **11**, 40232 (2019).
7. Takashima, K., Yoshinaka, K., Okazaki, T. & Ikeuchi, K. An endoscopic tactile sensor for low invasive surgery. *Sens. Actuators A: Phys.* **119**, 372 (2005).
8. Sun, H. et al. Highly stretchable, transparent, and bio-friendly strain sensor based on self-recovery ionic-covalent hydrogels for human motion monitoring. *Macromol. Mater. Eng.* **304**, 1900227 (2019).
9. Sundaram, S. et al. Learning the signatures of the human grasp using a scalable tactile glove. *Nature* **569**, 698 (2019).
10. Griffiths, D. J. *Introduction to Electrodynamics* 405–407 (Pearson Education, 2012).
11. Orfanidis, S. J. *Electromagnetic Waves & Antennas* 242 (Rutgers University Press, Rutgers, 2016).
12. Feng, P. et al. Ionic liquids-filled patterned cavities improve transmittance of transparent and stretchable electronic polydimethylsiloxane films. *J. Mater. Sci.* **54**, 11134 (2019).
13. Ruth, S. R. A. & Bao, Z. Designing tunable capacitive pressure sensors based on material properties and microstructure geometry. *ACS Appl. Mater. Inter.* **12**, 58301 (2020).
14. Jung, M. et al. Transparent and flexible Mayan-pyramid-based pressure sensor using facile-transferred indium tin oxide for bimodal sensor applications. *Sci. Rep.* **9**, 14040 (2019).
15. Luo, S. et al. Tunable-sensitivity flexible pressure sensor based on graphene transparent electrode. *Solid State Electron* **145**, 29 (2018).
16. Choi, H. B. et al. Transparent pressure sensor with high linearity over a wide pressure range for 3D touch screen applications. *ACS Appl. Mater. Inter.* **12**, 16691 (2020).
17. Kim, H. et al. Transparent, flexible, conformal capacitive pressure sensors with nanoparticles. *Small* **14**, 1703432 (2018).
18. Nie, B., Xing, S., Brandt, J. D. & Pan, T. Droplet-based interfacial capacitive sensing. *Lab. Chip.* **12**, 1110 (2012).
19. Nie, B., Li, R., Cao, J., Brandt, J. D. & Pan, T. Flexible transparent iontronic film for interfacial capacitive pressure sensing. *Adv. Mater.* **27**, 6055 (2015).
20. Zhang, X. et al. P-141: Research on the improvements of invisibility of metal mesh touch panel and influencing factors. *SID Int. Symp. Dig. Tech. Pap.* **50**, 1755 (2019).
21. Chen, L. et al. PDMS-based capacitive pressure sensor for flexible transparent electronics. *J. Sens.* **2019**, 1418374 (2019).
22. Yu, X. et al. Investigation of light transmission and scattering properties in silver nanowire mesh transparent electrodes. *Mater. Lett.* **145**, 219 (2015).
23. Tang, R. et al. Flexible pressure sensors with microstructures. *Nano Select* https://doi.org/10.1002/nano.202100003 (2021).
24. Jackson, R. L. & Green, I. A finite element study of elasto-plastic hemispherical contact against a rigid flat. *J. Tribol.-T Asme* **127**, 343 (2005).
25. Nie, B., Li, R., Brandt, J. D. & Pan, T. Iontronic microdroplet array for flexible ultrasensitive tactile sensing. *Lab Chip* **14**, 1107 (2014).
26. Popov, V. L. (ed) *Contact Mechanics and Friction: Physical Principles and Applications* 55 (Springer, 2010).
27. Calado, M. S. et al. Electrolytic conductivity of four imidazolium-based ionic liquids. *Int. J. Thermophys.* **34**, 1265 (2013).
28. Tomiyasu, H. et al. An aqueous electrolyte of the widest potential window and its superior capability for capacitors. *Sci. Rep.* **7**, 45048 (2017).
29. Winterton, N. Solubilization of polymers by ionic liquids. *J. Mater. Chem.* **16**, 4281 (2006).
30. Parsons, R. The electrical double layer: Recent experimental and theoretical developments. *Chem. Rev.* **90**, 813 (1990).
31. Butt, H. & Kappl, M. *Electrostatic Double-Layer Forces, Surface, and Interfacial Forces*. 93–125 (Wiley-VCH Verlag GmbH & Co. KgaA, 2010).
32. Pang, L. et al. Enhanced pressure & proximity sensitivities of a flexible transparent capacitive sensor with PZT nanowires. *IOP Conf. Ser.: Mater. Sci. Eng.* **479**, 12035 (2019).
33. Daniels, P. H. A brief overview of theories of PVC plasticization and methods used to evaluate PVC-plasticizer interaction. *J. Vinyl Addit. Technol.* **15**, 219 (2009).
34. Kiran Kumar, A. B. V., Wan Bae, C., Piao, L. & Kim, S. Silver nanowire based flexible electrodes with improved properties: High conductivity, transparency, adhesion and low haze. *Mater. Res. Bull.* **48**, 2944 (2013).
35. Zhao, D., Zhang, G., Zhang, X. & Li, D. Optical properties of paraffin at temperature range from 40 to 80 °C. *Optik* **157**, 184 (2018).
36. Li, S. et al. All-in-one iontronic sensing paper. *Adv. Funct. Mater.* **29**, 1807343 (2019).
37. Li, R. et al. Supercapacitive iontronic nanofabric sensing. *Adv. Mater.* **29**, 1700253 (2017).
38. Li, S., Chu, J., Li, B., Chang, Y. & Pan, T. Handwriting iontronic pressure sensing origami. *ACS Appl. Mater. Inter.* **11**, 46157–46164 (2019).
39. Zhu, Z., Li, R. & Pan, T. Imperceptible epidermal-iontronic interface for wearable sensing. *Adv. Mater.* **30**, 1705122 (2018).
40. Huang, S., Li, M., Shen, L., Qiu, J. & Zhou, Y. Flexible fabrication of biomimetic compound eye array via two-step thermal reflow of simply pre-modeled hierarchic microstructures. *Opt. Commun.* **393**, 213 (2017).
41. Lin, T., Yang, H. & Chao, C. Concave microlens array mold fabrication in photoresist using UV proximity printing. *Microsyst. Technol.* **13**, 1537 (2007).
42. Li, R., Nie, B., Digiglio, P. & Pan, T. Microflotronics: A flexible, transparent, pressure-sensitive microfluidic film. *Adv. Funct. Mater.* **24**, 6195 (2014).
43. Yu, Z. & Wu, P. Underwater communication and optical camouflage Ionogels. *Adv. Mater.* **33**, 2008479 (2021).
44. Yoo, J. et al. Industrial grade, bending-insensitive, transparent nanoforce touch sensor via enhanced percolation effect in a hierarchical nanocomposite film. *Adv. Funct. Mater.* **28**, 1804721 (2018).
45. Shi, R., Lou, Z., Chen, S. & Shen, G. Flexible and transparent capacitive pressure sensor with patterned microstructured composite rubber dielectric for wearable touch keyboard application. *Sci. China Mater.* **61**, 1587 (2018).
46. Lai, J. et al. Highly stretchable, fatigue-resistant, electrically conductive, and temperature-tolerant Ionogels for high-performance flexible sensors. *ACS Appl. Mater. Inter.* **11**, 26412 (2019).
47. Kim, K. K. et al. Transparent wearable three-dimensional touch by self-generated multiscale structure. *Nat. Commun.* **10**, 2582 (2019).
48. Hoque, M., Fairhurst, M & Howells, G. Evaluating biometric encryption key generation using handwritten signatures. In *2008 Bio-Inspired, Learning, and Intelligent Systems for Security*. Edinburgh, UK 17–22 (2008).
49. Dacosta, R. S., Wilson, B. C. & Marcon, N. E. New optical technologies for earlier endoscopic diagnosis of premalignant gastrointestinal lesions. *J. Gastroenterol. Hepatol.* **17**, S85 (2002).
50. Ren, H. et al. Transfer-medium-free nanofiber-reinforced graphene film and applications in wearable transparent pressure sensors. *ACS Nano* **13**, 5541 (2019).
51. Linyong, S., Jinwu, Q., Zhen, Z., Yanan, Z. & Jinxi, Y. In *Proceedings of the Sixth IEEE CPMT Conference on High Density Microsystem Design and Packaging and Component Failure Analysis* (HDP '04) 181–184 (IEEE, 2004).
52. Lee, H. et al. An endoscope with integrated transparent bioelectronics and theranostic nanoparticles for colon cancer treatment. *Nat. Commun.* **6**, 10059 (2015).
53. Guimaraes, C. F., Gasperini, L., Marques, A. P. & Reis, R. L. The stiffness of living tissues and its implications for tissue engineering. *Nat. Rev. Mater.* **5**, 351 (2020).
54. Chuang, C. H., Li, T. H., Chou, I. C. & Teng, Y. J. Piezoelectric tactile sensor for submucosal tumor hardness detection in endoscopy. In *18th Int. Conf. Solid-State Sensors, Actuators, and Microsystems (Transducers)*, 871–875 (IEEE, 2015).
55. Zhang, Y., Wei, X., Yue, W., Zhu, C. & Ju, F. A dual-mode tactile hardness sensor for intraoperative tumor detection and tactile imaging in robot-assisted minimally invasive surgery. *Smart Mater. Struct.* **30**, 85041 (2021).
56. Hertz, D. L. & Farinella, A. C. Shore a Durometer and Engineering Properties. *Presented at the Fall Technical Meeting of The New York Rubber Group*, 1–13 (New York, 1998).
57. Sugimoto, M. et al. What is the nature of pancreatic consistency? Assessment of the elastic modulus of the pancreas and comparison with tactile sensation, histology, and occurrence of postoperative pancreatic fistula after pancreaticoduodenectomy. *Surgery* **156**, 1204 (2014).
58. Nabavizadeh, A. et al. Noninvasive Young's modulus visualization of fibrosis progression and delineation of pancreatic ductal adenocarcinoma (PDAC) tumors using Harmonic Motion Elastography (HME) in vivo. *Theranostics* **10**, 4614 (2020).

59. Scardulla, F. et al. Study on the effect of contact pressure during physical activity on photoplethysmographic heart rate measurements. *Sensors* **20**, 5052 (2020).
60. Wallberg-Jonsson, S., Caidahl, K., Klintland, N., Nyberg, G. & Rantapaa-Dahlqvist, S. Increased arterial stiffness and indication of endothelial dysfunction in long-standing rheumatoid arthritis. *Scand. J. Rheumatol.* **37**, 1 (2008).

ACKNOWLEDGEMENTS

This research was supported by the Joint Research Fund for Overseas Chinese Scholars and Scholars in Hong Kong and Macao (51929501), the National Natural Science Foundation of China (62001461), the Program for Guangdong Innovative and Entrepreneurial Teams (2016ZT06D631), the Natural Science Foundation of Guangdong Province (2019A1515010796), the Shenzhen Engineering Laboratory of Single-molecule Detection and Instrument Development (XMHT20190204002), the Shenzhen Fundamental Research Program (JCYJ20180305180923182 and JCYJ20170413164102261). The authors thank Xiuli Xu, Zongyin Hu from Shenzhen Institutes of Advanced Technology, Chinese Academy of Science, and Hong Ye from Tacsense. Inc. for their supports on the hardware and software designs of the TIS system. The authors will also thank Prof. Qi Tong and Prof. Yi Gong from Fudan University for their supports on the mechanical theory analysis of the TIS device, Prof. Yuhang Chen and Prof. Baoqing Li from University of Science and Technology of China for their supports on the optical theory analysis of the TIS device.

AUTHOR CONTRIBUTIONS

T.P., Y.C., and Z.G.Y. conceptualized the idea, directed the study, and supported the project. J.T. and Y.C. fabricated and characterized the devices, as well as analyzed the data. C.Z. and Q.L. conducted the human tissue experiments. J.T. contributed to writing the manuscript, T.P. and Y.C. revised the manuscript.

COMPETING INTERESTS

Y.C. and T.P. are involved with TacSense, Inc., which is developing iontronic sensing technologies for medical and industrial applications.

ADDITIONAL INFORMATION

Supplementary information The online version contains supplementary material available at https://doi.org/10.1038/s41528-022-00162-y.

Correspondence and requests for materials should be addressed to Yu Chang, Zhenguo Yang or Tingrui Pan.

Reprints and permission information is available at http://www.nature.com/reprints

Publisher's note Springer Nature remains neutral with regard to jurisdictional claims in published maps and institutional affiliations.